Research Article

A numerical investigation of the species transport approach for modeling of gaseous combustion

Upendra RAJAK[1]⊙, **Prerana NASHINE**[2]⊙, **Prem KUMAR CHAURASIYA**[3]⊙,
Tikendra NATH VERMA[4]⊙

¹Department of Mechanical Engineering, Rajeev Gandhi Memorial College of Engineering and Technology Nandyal-518501, India
²Department of Mechanical Engineering, Sagar Institute of Science and Technology Gandhi Nagar, Bhopal, M.P, India
³Department of Mechanical Engineering, Sagar Institute of Science and Technology Gandhi Nagar, Bhopal, M.P, India
⁴Department of Civil Engineering, Madan Mohan Malaviya University of Technology Technical University Gorakhpur- 273016, India
⁵Department of Mechanical Engineering, Maulana Azad National Institute of Technology Bhopal-462003, India

ARTICLE INFO

ABSTRACT

This present work shows a study of the effect of thermal radiation in the simulation of a turbulent, non-premixed diesel-air, hydrogen-air, kerosene-air, n-butanol, pentane-air, propane-air and methane–air used in a 2D geometry cylindrical combustion chamber. The numerical simulation based on the solution of the mass, momentum, energy and the chemical species conservation equations was performed for steady state condition using Computation Fluid Dynamic (CFD), while the turbulence modeling was considered via standard k–ε model. The results indicate that highest mass fraction of NO emissions with hydrogen-air fuel compared to diesel fuel. The results showed a better performance of kerosene-air alternative based on the emissions characteristics in the present work. The CO_2 emission reduced with hydrogen-air compared to diesel fuel due to better combustion. A significant decrease of emissions characteristics (O_2, H_2O and NO) was observed. The present numerical investigated results of methane-air are compared to experimental results compared to Silva et al. (2007) and Garreton and Simonin (1994) for tool validation.

Cite this article as: Rajak U, Nashine P, Chaurasiya PK, Verma TN. A numerical investigation of the species transport approach for modeling of gaseous combustion. J Ther Eng 2021;7(Supp 14):2054–2067.

*Corresponding author.
*E-mail address: upendrarajak86@gmail.com; verma.tikks@gmail.com

*This paper was recommended for publication in revised form by
Regional Editor Baha Zafer*

INTRODUCTION

Emissions of nitric oxides, unburned hydrocarbons, carbon monoxides, particulate matter and soot produced by the compression ignition (CI) engines have been restrained pointedly over the past few years. In previous years, researchers have tried to minimize the emissions and increase the thermal efficiency of the CI engines. Now a days, minimizing the emissions from the engine and improving the thermal efficacy of CI engines are the critical challenge for the industrialized world and developing countries [1–2].

The effect of natural gas energy shared with diesel fuel, operating with various injection timing and evaluated the engine characteristics has been investigated. The results showed that the maximum indicated thermal efficiency at 12–20.0° C TDC with 50.0% natural gas energy share and nitrogen oxide (NO_x) emission decreases with 60.0% natural gas energy shares [3]. The effect of two-stage injection approach on diesel engine characteristics using AVL Fire CFD code were simulated. The results showed that increasing the two-stage injection reduced the ISFC and NO_x emissions, while slight effect on soot, HC and CO emissions for pilot injection [4]. The effect of alternative fuel on diesel engine by 3-D CFD simulation code has been investigated. The CFD results shows the increase in fraction of alternative fuel decreases CO emission [5]. The effect of combustion characteristics on diesel engine fuelled with alternative mixture (Rapeseed and Sunflower) using 3-D CFD simulation code were evaluated and result showed a reduction in soot emissions for alternative mixture compared to diesel fuel [6]. The effect of multiple inoculation on diesel engine characteristics using natural gas–diesel fuel mixture were experimentally and numerically investigated. The results showed that the thermal efficiency and NO_x emissions first increased and then reduced with advanced first diesel injection timing. The pressure rise rate per degree, CO and CH4 emissions was first reduced and then improved with advanced first diesel injection timing. Moreover, a reduction in CO and CH4 emissions with increase in first diesel injection ratio was observed [7].

The effects of alternative fuel (coconut, palm and soybean methyl ester)-diesel fuel emulsion and compared to diesel fuel on light-duty diesel engine by using 3-D CFD code were simulated. The results showed the improved thermal NO emissions with higher fraction of soybean methyl ester due to higher combustion temperature [8]. The effect of thermal radiation of a 2-D axisymmetric turbulent, non-premixed methane–air flame using 3-D CFD code were simulated. The results showed the importance of thermal radiation for an accurate prediction of the thermal behaviour [9]. The researchers observed that with addition of hydrogen to a jet fuel on lab-scale furnace with slot type burner, there is decrease in flame length with an increase in hydrogen fraction into jet fuel. However, the time-average mean temperature decreases with an increase hydrogen fraction into jet fuel [10]. The effect of addition of biodiesel to combustion fuel with varying high temperature (1100–2100 k) for diesel fuel at 2100 K and biodiesel at 1100 K were evaluated [11].

The effects of variations in H2O to CO2 molar-ratio has been investigated using weighted-sum-of-grey-gases (WSGG) model and compared grey models by 3-D CFD code. The results were better when engine operates at temperature (500–2500 K), pressure path-lengths (0.01–60 bar) and molar-ratio (0.125–2.0) [12]. Demonstrated the effect of Eulerian PDF transport method for evaluating the influence in stabilized hydrocarbon flames (Sandia Flame D (SFD) and Delft Flame III) with the non-gray radiation modeling using WSGG method. The result showed the lower value (micro-mixing constant equal 2) of stable flame, when SFD was used and predicts better results at micro-mixing constant equal to 3. The mass fraction of NO was found to be over predicted by 70% with micro-mixing constant equal to 3 and an over prediction of another 25% when the Cu increased to 4.0.

In this study, theoretical combustion analysis and CFD simulation of six different fuels of diesel-air, hydrogen-air, kerosene-air, n-butanol, pentane-air and propane-air was used in a 2D geometry cylindrical combustion chamber, without considering the thermal radiation effect using Fluent and compared with diesel combustion. Results are compared with diesel fuel and an appropriate blend ratio of biodiesel is suggested for maximum utility from this study.

THEORETICAL FORMULATION OF MODELS

In the present investigation, k-epsilon turbulence model is selected for numerical analysis. The k-epsilon two equation turbulence model classified are Standard k-epsilon, RNG k-epsilon and Realizable k-epsilon to solve energy transport equation, mass conservation equation, continuity equation, energy conservation equation and the result showed that k-epsilon standard turbulent model perform better [8–9, 11, 13].

Mass Conservation Equation

The equation used for conservation of mass, or continuity equation calculation mass-averaged temperature and area-average velocity will be computed at outlet of the cylindrical combustion chamber the given equation of the cylindrical combustion chamber.

$$\frac{\partial \rho}{\partial t} + \nabla . (\rho \vec{v}) = S_m \qquad (1)$$

This equation is general form of the mass conservation equation and is valid for incompressible as well as

compressible flows. For 2D axisymmetric geometries, the continuity equation is given by:

$$\frac{\partial \rho}{\partial t} + \frac{\partial}{\partial x}(\rho v_x) + \frac{\partial}{\partial r}(\rho v_r) + \frac{\rho v_r}{r} = S_m \quad (2)$$

Momentum Equation

Conservation of momentum in an inertial (non-accelerating) reference frame is described by:

$$\frac{\partial}{\partial t}(\rho \vec{v}) + \nabla \bullet (\rho \vec{v} \vec{v}) = \nabla \bullet p + \nabla \bullet (\overline{\overline{\tau}}) + \rho \vec{g} + \vec{F} \quad (3)$$

For 2D axisymmetric geometries, the axial and radial momentum conservation equations are given by:

$$\frac{\partial}{\partial t}(\rho v_x) + \frac{1}{r}\frac{\partial}{\partial x}(r\rho v_x v_x) + \frac{1}{r}\frac{\partial}{\partial r}(r\rho v_r v_x) = -\frac{\partial p}{\partial x} + F_x \quad (4)$$

$$\frac{\partial}{\partial t}(\rho v_r) + \frac{1}{r}\frac{\partial}{\partial x}(r\rho v_x v_r) + \frac{1}{r}\frac{\partial}{\partial r}(r\rho v_r v_r) = -\frac{\partial p}{\partial x} + F_r \quad (5)$$

Energy Conservation Equation

Conservation of energy is represented as [23]:

$$\frac{\partial}{\partial t}(\rho E) + \nabla \bullet (\vec{v}(\rho E + p)) = \nabla \bullet \left(\sum_j h_j J_j\right) + S_h \quad (6)$$

Turbulence Model

Two-equation turbulence model was allowed to determine a turbulent length and time scale by solving two separate transport equations.

Transport Equations for the Standard Model

The turbulence kinetic energy, k and its rate of dissipation, are obtained from the following transport equations.

$$\frac{\partial}{\partial t}(\rho k) + \frac{\partial}{\partial x_i}(\rho k u_i) = \frac{\partial}{\partial x_j}\left[\left(\mu + \frac{\mu_t}{\sigma_k}\right)\frac{\partial k}{\partial x_j}\right] + G_K \quad (7)$$
$$+ G_b - \rho\varepsilon - Y_M + S_K$$

$$\frac{\partial}{\partial t}(\rho\varepsilon) + \frac{\partial}{\partial x_i}(\rho\varepsilon u_i) = \frac{\partial}{\partial x_j}\left[\left(\mu + \frac{\mu_t}{\sigma_\varepsilon}\right)\frac{\partial\varepsilon}{\partial x_j}\right]$$
$$+ C_{1\varepsilon}\frac{\varepsilon}{K}\left(G_K + C_{3\varepsilon}G_b\right) \quad (8)$$
$$- C_{2\varepsilon}\rho\frac{\varepsilon^2}{K} - Y_M + S_\varepsilon$$

The Eddy Breakup–Arrhenius Chemical Reactions Model

It is considered that the global chemical reactions steps concerning the following species: methane, water vapor, oxygen, nitrogen, carbon monoxide and carbon dioxide. A conservation equation is essential for all the species. The following conservation equation for the α-th chemical species [9, 13]:

$$\overline{u}\frac{\partial}{\partial x}(\rho\overline{f_\alpha}) + \overline{v}\frac{\partial}{\partial r}(\rho\overline{f_\alpha}) = \vec{\nabla}\bullet\left(\left(\rho D + \frac{\mu_t}{Sc_t}\right)\vec{\nabla}\overline{f_\alpha}\right) + R_\alpha \quad (9)$$

D mixture mass diffusivity
Sc_t Schmidt turbulent number
$\overline{f_\alpha}$ average mass fraction of the α-th chemical specie
$\overline{R_\alpha}$ Average volumetric rate of formation or destruction of the α-th chemical specie.

Wall Function

The dependent wall function is used to determine temperature and velocity profile near about the wall using equation as follows [14].

In the laminar boundary layer theory ($Y^+ \leq 11.63$)

$$U^+ = Y^+ \quad (10)$$

$$T^+ = \sigma_e U^+ \quad (11)$$

In the turbulent boundary layer theory ($Y^+ > 11.63$)

$$U^+ = \frac{1}{k}\ln\left(E_y^+\right) \quad (12)$$

$$T^+ = \sigma_{e,t}\left[U^+ + R\left(\frac{\sigma_e}{\sigma_e},t\right)\right] \quad (13)$$

In the above equation, R is a viscous sub layer thermal resistance factor and Y^+, U^+ and T^+ are dimensionless parameters distance from the wall, non-tangential velocity and temperature respectively.

$$U^+ = \frac{U^*}{U_T} \quad (14)$$

$$Y^+ = \frac{YU_T}{v} \quad (15)$$

Table 1. The k-ε Turbulence Model Constant [9, 13]

Constant	$C_{1\varepsilon}$	$C_{2\varepsilon}$	C_μ	C_2	σ_ε	σ_k
Standard Model	1.44	1.92	0.09	–	1.3	1.0

Table 2. Boundary layer theory constant

Constant	Values
K_v	0.41
E	9.0
$\sigma_{e,t}$	0.90

$$T^+ = \left(\frac{\rho U_T}{q_w}\right) C_p T \ln\left(\frac{T_w}{T}\right) \quad (16)$$

$$U_T = \sqrt{\frac{\tau_w}{\rho}} \quad (17)$$

Performance Parameter

The equation used for determining mass-averaged temperature at outlet of the cylindrical combustion chamber can be written as [9, 13, 15].

$$\overline{T} = \frac{\int T \rho \overline{v}.d\overline{A}}{\int \rho \overline{v}.d\overline{A}} \quad (18)$$

The equation used for calculating area-weighted velocity-magnitude average at outlet of the cylindrical combustion chamber. And it is represented by equation below [15].

$$\overline{v} = \frac{1}{A}\int v dA \quad (19)$$

Modelling of the Problem Numerical Simulation

In present case, the numerical simulation is carried out in a cylindrical combustion chamber having 45.0 cm diameter and 180.0 cm length [11, 13, and 15]. The geometric modelling of 2D cylinder combustion chamber is done in workbench as shown in Figure (a, b). In present case, area weighted average velocity and mass-weighted average temperature, mass fraction of species and NO_X emission at outlet of cylindrical combustion chamber are carried out. The pressure-based solver, absolute velocity formation and steady state numerical simulation is taken at inlet boundary conditions, given in Table-1. The wall of combustion chamber is assumed to be smooth with no slip condition. The k-epsilon standards two equations, turbulence model and species transport are used for simulation [13]. The flame used in this case is turbulence diffusion flame and small nozzle in the center of the cylindrical combustion chamber at the inlet of fuel. In all the cases, a small size fuel nozzle in the center of the cylindrical combustion chamber, inlet velocity magnitude (80.0 m/s) of fuel at a temperature of 300.0 K and inlet velocity magnitude (0.5 m/s) of air at 300.0 K into cylindrical combustion chamber are considered. The diameter of fuel inlet cylindrical is 0.5 cm and the diameter of air enter cylindrical combustion chamber is 22.5 cm.

Computational Model Validation

To validate the CFD model [24], the experimental and simulation results were compared with previous literature 2-D combustion geometry, which is shown in Figure 1. The
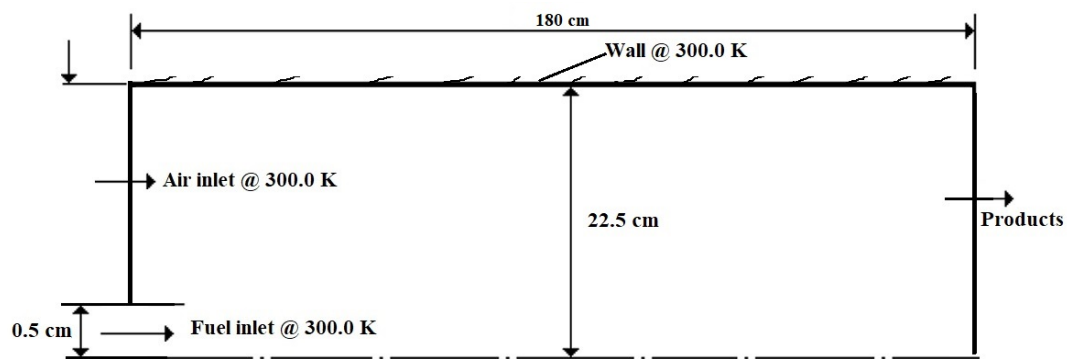
(a)

(b)

Figure 1. (a) Input and output from combustion chamber. (b) Input and output from combustion chamber with reaction.

Table 3. Input and output boundary conditions for simulation [11, 13, 15]

Component	Values
Inlet velocity of Fuel (m/s)	80.0
Inlet velocity of air (m/s)	0.5
Inlet Initial gauge Pressure (Pascal)	0.0
Wall temperature (K)	300.0
Inlet temperature (K)	For air (300.0 K) & Fuel (300.0 K)
Turbulent intensity (%)	10
Outlet initial gauge pressure (Pascal),	0.0
Temperature (K)	300.0 K
Wall temperature (K)	300.0 K

Figure 2. 2D cylindrical combustion mesh.

tetrahedral meshing of cylindrical combustion chamber flow domain is generated in ANSYS Workbench. The size and shape of mesh element affects the accuracy of result. Only partial section of the combustion geometry is meshed in ANSYS Workbench. The comparisons of the 2-D combustion geometry, mass of fuel injected, constant specific heat with equivalence ratio (0.75) are kept constant for whole set of simulations.

mesh file is shown in Figure 2 and tool validation for methane-air fuel at same operating condition is shown in Figure 3. The results shows a good agreement between the experimental and numerical results for 2-D combustion geometry. The CFD model is able to predict the combustion temperature, NO emission, CO_2 emission, etc. The mesh is created by using the ANSYS [11]. Workbench cylindrical combustion chamber model is taken for numerical simulation. The numerical simulation carried out for different gaseous fuel used in this study are diesel, hydrogen, kerosene, n-butanol, pentane, propane and methane-air fuel at constant specific heat with equivalence ratio (0.75). The 2-D geometry cylindrical combustion chamber, velocity, temperature, CO_2, H_2O, O_2, NOX contour and mass fraction of CO_2, H_2O, O_2, NOX emissions and turbulent kinetic energy were found within the combustion processes. The

RESULTS AND DISCUSSION

Temperature Distribution in the Combustion Chamber

Temperature contours for diesel, hydrogen, kerosene, n-butanol, pentane and propane determined by the species transport model are shown in Figure 4 (a). Absolute difference of the temperature contours for all tested fuels at same operating conditions are shown in Figure 4 (b). Temperature was found to be higher for hydrogen fuel (3800.0 K) as compared to other tested fuels. The higher combustion temperature leads to higher NOX emissions [11]. The combustion chamber temperature is higher at the near combustion axis for all the fuels as per temperature contours. The combustion temperature profile fluctuates from 1700 to 2630 K for diesel fuel, 1880 to 3800 K for hydrogen fuel, 1690 to 3500 K for kerosene, 1890 to 2950
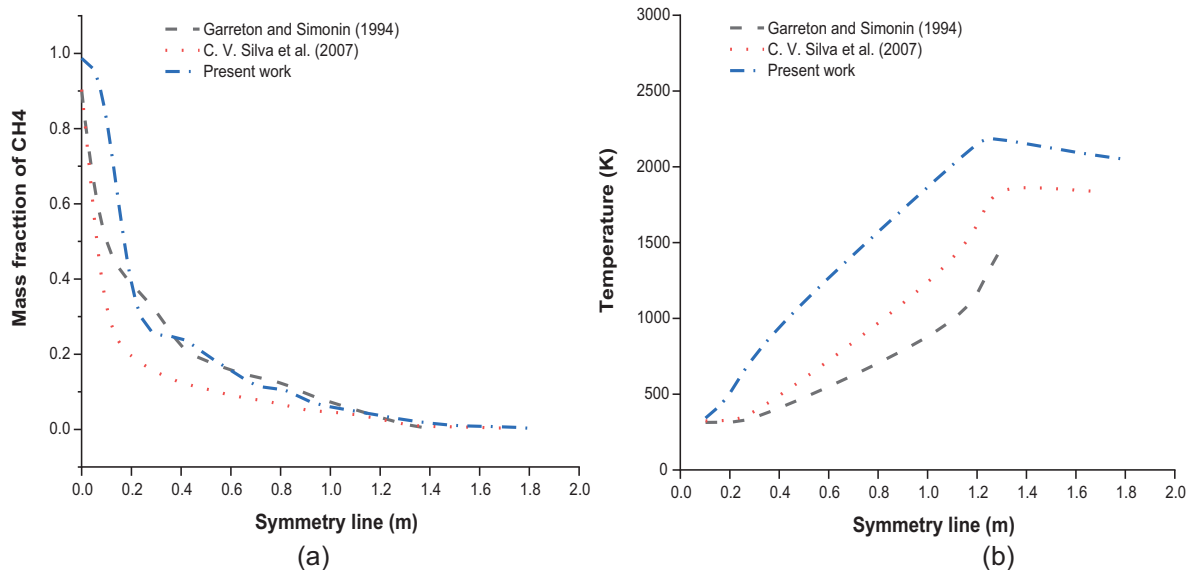
Figure 3. (a) Mass fraction of CH_4 and (b) combustion temperature variation with symmetry line.

(a)

(b)
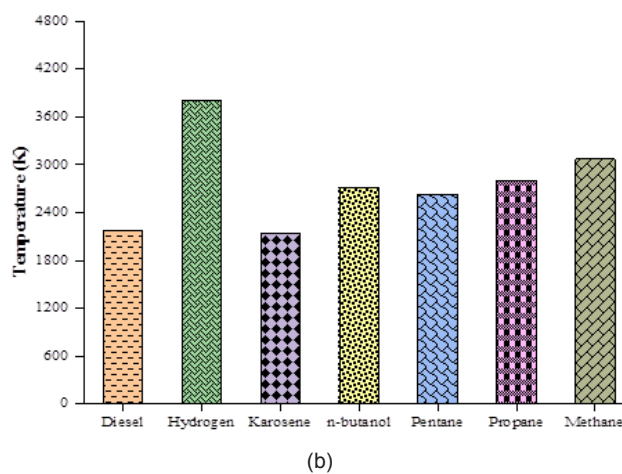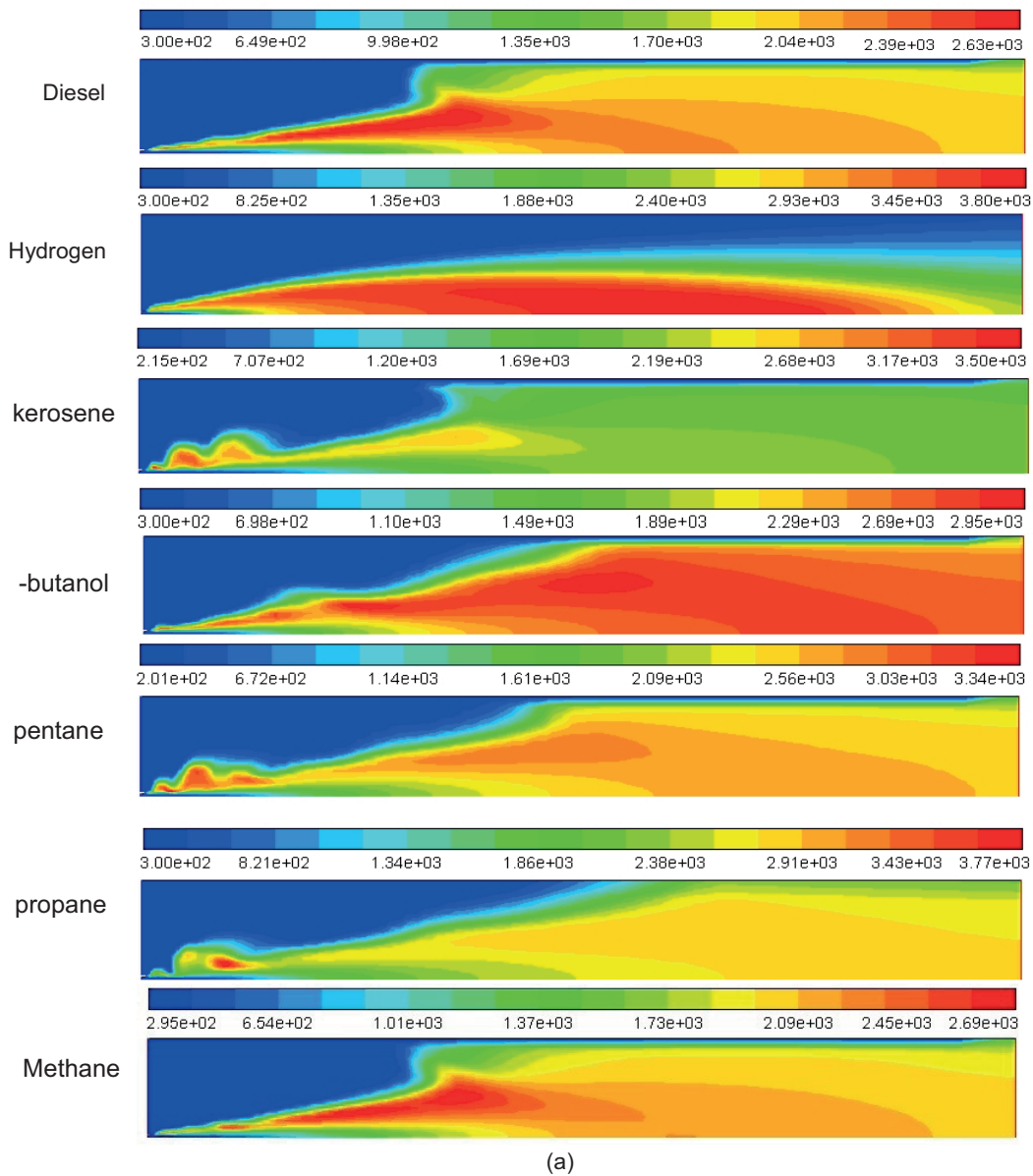
Figure 4. (a) Contours of temperature inside domain with no radiation for diesel, hydrogen, kerosene, n-butane, pentane, propane and methane. (b) Maximum temperature versus symmetry line for diesel, hydrogen, kerosene, n-butane, pentane, propane and methane.

K for n-butanol, 2560 to 3340 K for pentane and 1860 to 2910 K for propane, while kerosene alternative fuel showed lower combustion temperature due to effects of oxygen contents [31].

NO Pollutant Distribution in the Combustion Chamber

NO pollutant contours for diesel, hydrogen, kerosene, n-butanol, pentane and propane determined by the species transport model are shown in Figure 5 (a). Absolute differences of the temperature contours for all tested fuels at same operating conditions are shown in Figure 5 (b). Prompt and thermal formation of NO emissions was found to be higher for hydrogen fuel and lower for diesel fuel compared to other tested fuels. The higher combustion temperature leads to higher NO_X emissions [11, 16–20]. In the combustion chamber, formations of NO emissions are higher at near to the combustion axis for all the fuels as per NO pollutant contours. In the combustion chamber, mass fraction of NO pollutant contours profile fluctuates from 0.00178 to 0.00395 for diesel fuel, 0.0147 to 0.0326 for hydrogen fuel, 0.00965 to 0.0214 for kerosene, 0.0075 to 0.0167 for n-butanol, 0.0285 to 0.0634 for pentane and 0.0155 to 0.0345, while in kerosene alternative fuel showed lowest mass fraction of NO pollutant. While, alternative fuels has higher mass fraction of NO emission during combustion fuel within the combustion chamber [25–28]. The NOX emission in combustion chamber was increased with increase in combustion temperature. An increase of NO_X emission in combustion is due to increasing after-burning temperature [26–27, 32].

Mass fraction of CO_2 emission

The CO_2 emission contours for diesel, hydrogen, kerosene, n-butanol, pentane and propane determined by the species transport model are shown in Figure 6 (a). Absolute difference of the CO_2 emission contours for all tested fuels at same operating conditions are shown in Figure 6 (b). The formation of CO_2 emission was found to be higher for n-butanol and pentane fuel and lower for kerosene and propane fuels compared to diesel fuel. In the combustion chamber formation of CO_2 emissions are highest at near the outlet for all the fuels as per CO_2 contours. The CO_2 emissions depends on viscosity, atomization processes, etc. [21–22, 29–30]. In the combustion chamber, mass fraction of CO_2 emission contours profile fluctuates from 0.103 to 0.127 for diesel fuel, almost nil for hydrogen fuel, 0.131 to 0.163 for kerosene, 0.113 to 0.189 for n-butanol, 0.144 to 0.192 for pentane and 0.138 to 0.172, while in hydrogen and kerosene alternative fuel showed lowest mass fraction of CO_2 emission than that of diesel fuel. Normally, carbon dioxides (CO_2) emission grows with the more fuel injection into the combustion chamber and advanced temperature with the exact ignition but hydrogen combustion resulted lesser amount of CO_2 emissions compared to diesel combustion fuel [31–33].

Mass fraction of O_2 pollutant

The mass fraction of O_2 emission contours for diesel, hydrogen, kerosene, n-butanol, pentane and propane determined by the species transport model are shown in Figure 7 (a). Absolute differences of the mass fraction O_2 emission contours for all tested fuels at same operating conditions are shown in Figure 7 (b). The formation of mass fraction O_2 emission was found to be higher for diesel fuel and lower for hydrogen fuel compared to other fuels. The formation of mass fraction of O_2 emissions is highest at the inlet for all the fuels as per mass fraction O_2 contours. In the combustion chamber, mass fraction of O_2 emission fluctuates from 0.173 to 0.231 for diesel fuel, 0.138 to 0.207 for hydrogen fuel, 0.175 to 0.234 for kerosene, 0.176 to 0.234 for n-butanol, 0.184 to 0.245 for pentane and 0.184 to 0.246, while in kerosene alternative fuel showed lowest mass fraction of O_2 emission than that of diesel fuel. This may be due to the growth of mass fraction of O_2 emission because of incomplete combustion process within the combustion chamber and advanced temperature with the exact ignition but hydrogen combustion showed fuel uniform result and methane-air combustion fuel showed higher amount of O_2 mass fraction emission compared to diesel combustion fuel [31–33].

Mass fraction of H_2O emission

The mass fraction H_2O emission contours for diesel, hydrogen, kerosene, n-butanol, pentane and propane determined by the species transport model are shown in Figure 8 (a). Absolute differences of the mass fraction of H2O emission contours for all tested fuels at same operating conditions are shown in Figure (b). The formation of mass fraction H_2O emission was found to be higher for n-butanol fuel and lower for kerosene fuel compared to other fuels. The formation of mass fraction H_2O emissions is highest at the outlet for all the fuels as per mass fraction H_2O contours. In the combustion chamber, mass fraction of H_2O emission was found to be 0.066 for diesel fuel, 0.246 for hydrogen fuel, 0.058 for kerosene, 0.0854 for n-butanol, 0.081 for pentane and 0.091, while in kerosene alternative fuel showed that lowest mass fraction of mass fraction H_2O emission than that of diesel fuel. This may be due to the growth of mass fraction of H_2O emission because of incomplete combustion process within the combustion chamber but mass fraction of H_2O for hydrogen combustion geometry resulted lesser amount of H_2O emission for methane-air fuel compared to diesel combustion fuel.

Turbulent kinetic energy

Turbulent kinetic energy (TKE) contours for diesel, hydrogen, kerosene, n-butanol, pentane and propane determined by the species transport model are shown in Figure 9 (a). Absolute differences of the TKE for all tested fuels at same operating conditions are shown in Figure 9 (b). The formation of TKE was found to be higher for
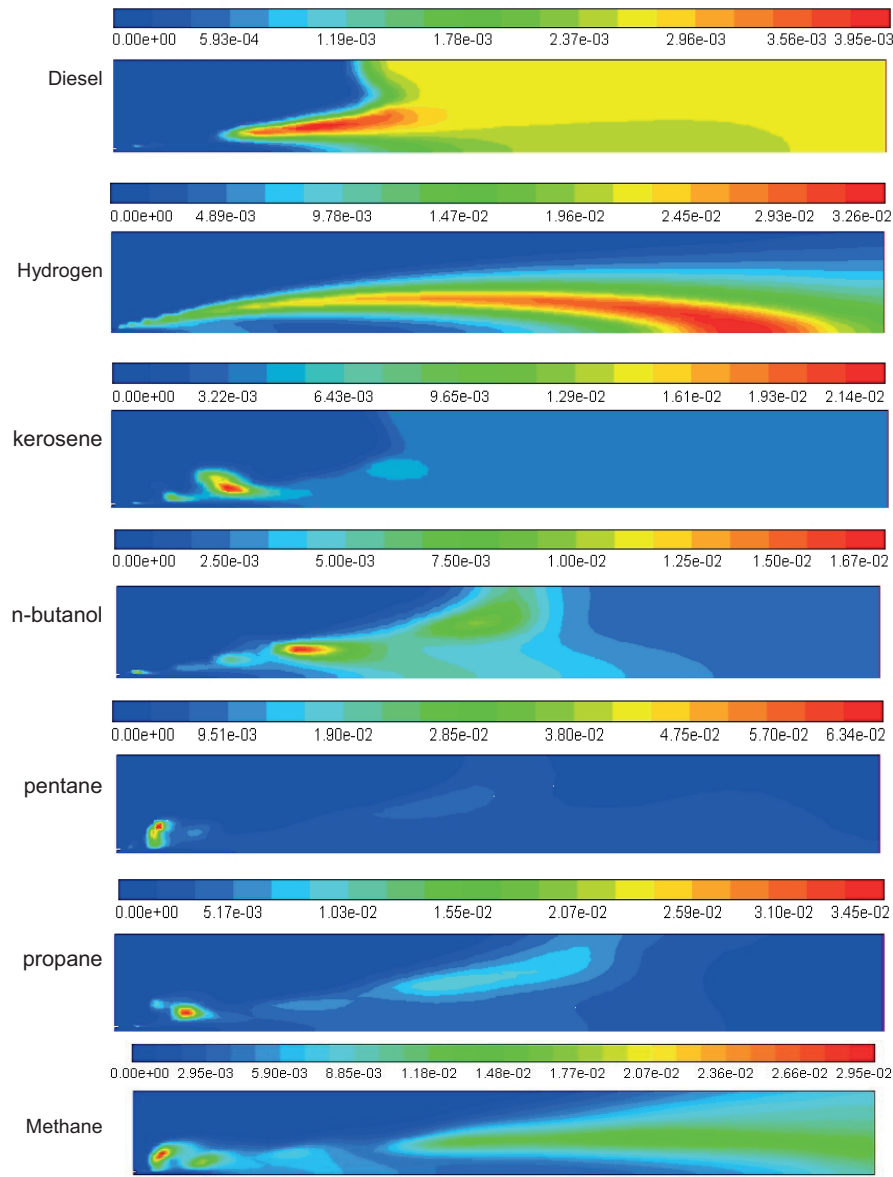
(a)
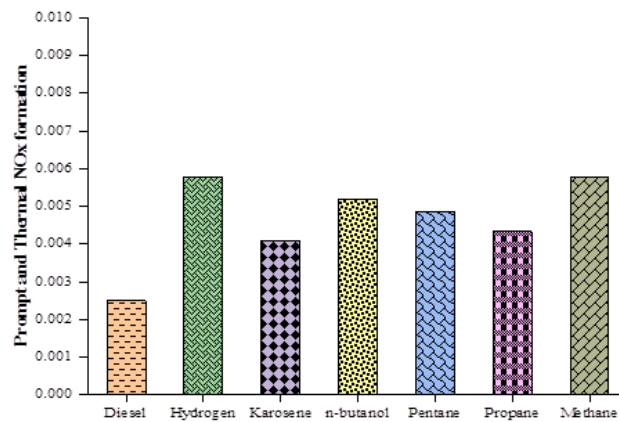
(b)

Figure 5. (a) Contours of NO pollutant inside domain with no radiation for diesel, hydrogen, kerosene, n-butane, pentane, propane and methane. (5) Peak NO pollutant distribution in the combustion chamber for diesel, hydrogen, kerosene, n-butane, pentane, propane and methane.
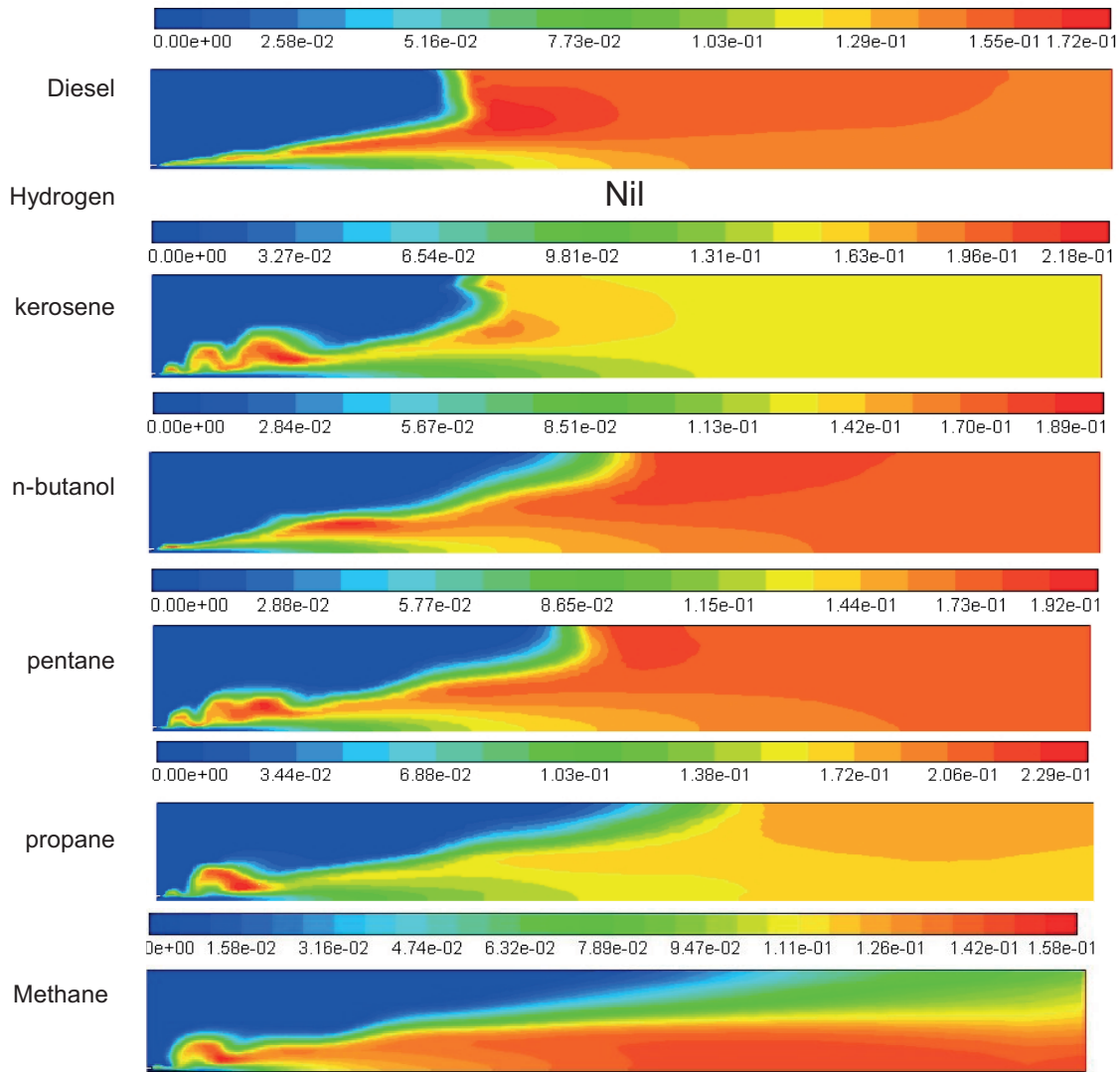
(a)
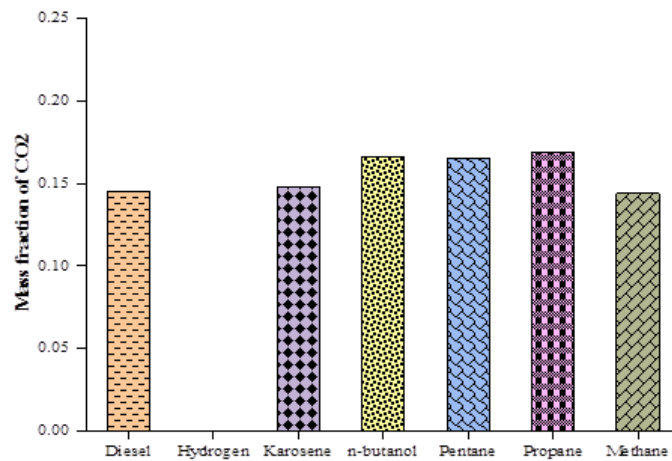
(b)

Figure 6. (a) Contours of CO_2 pollutant inside domain with no radiation for diesel, hydrogen, kerosene, n-butane, pentane, propane and methane. (b) Maximum mass fraction of CO_2 pollutant distribution in the combustion chamber for diesel, hydrogen, kerosene, n-butane, pentane, propane and methane.

(a)

(b)
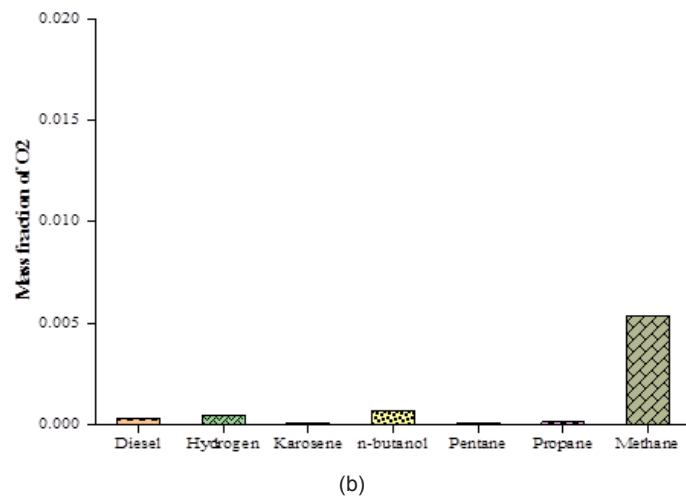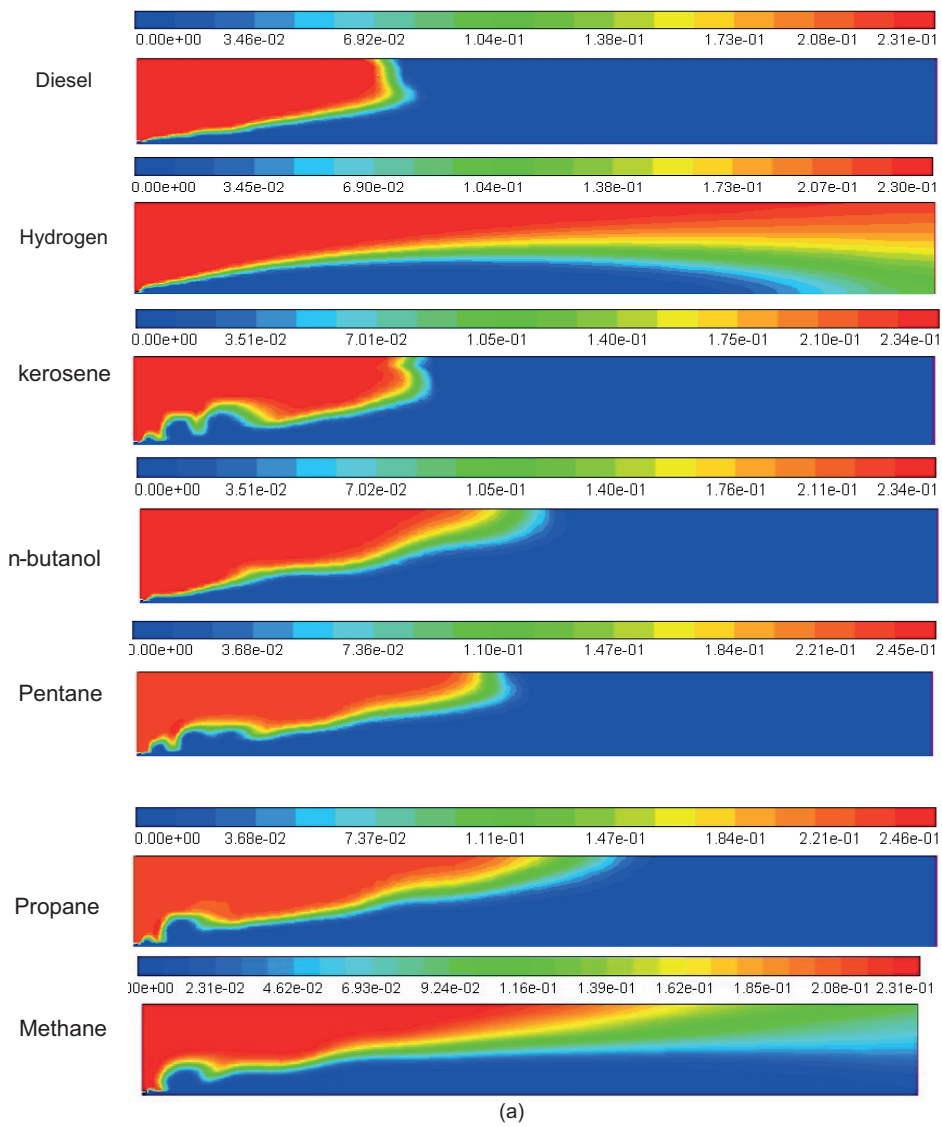
Figure 7. Contours of O_2 pollutant inside domain with no radiation for diesel, hydrogen, kerosene, n-butane, pentane, propane and methane. Maximum mass fraction of O_2 pollutant distribution in the combustion chamber for diesel, hydrogen, kerosene, n-butane, pentane, propane and methane.

(a)

(b)
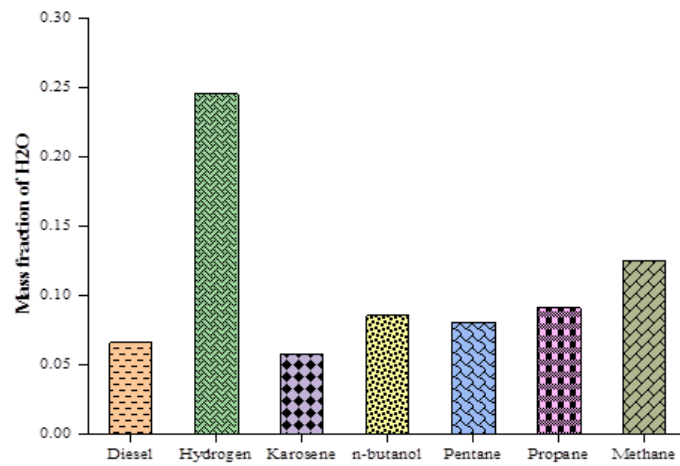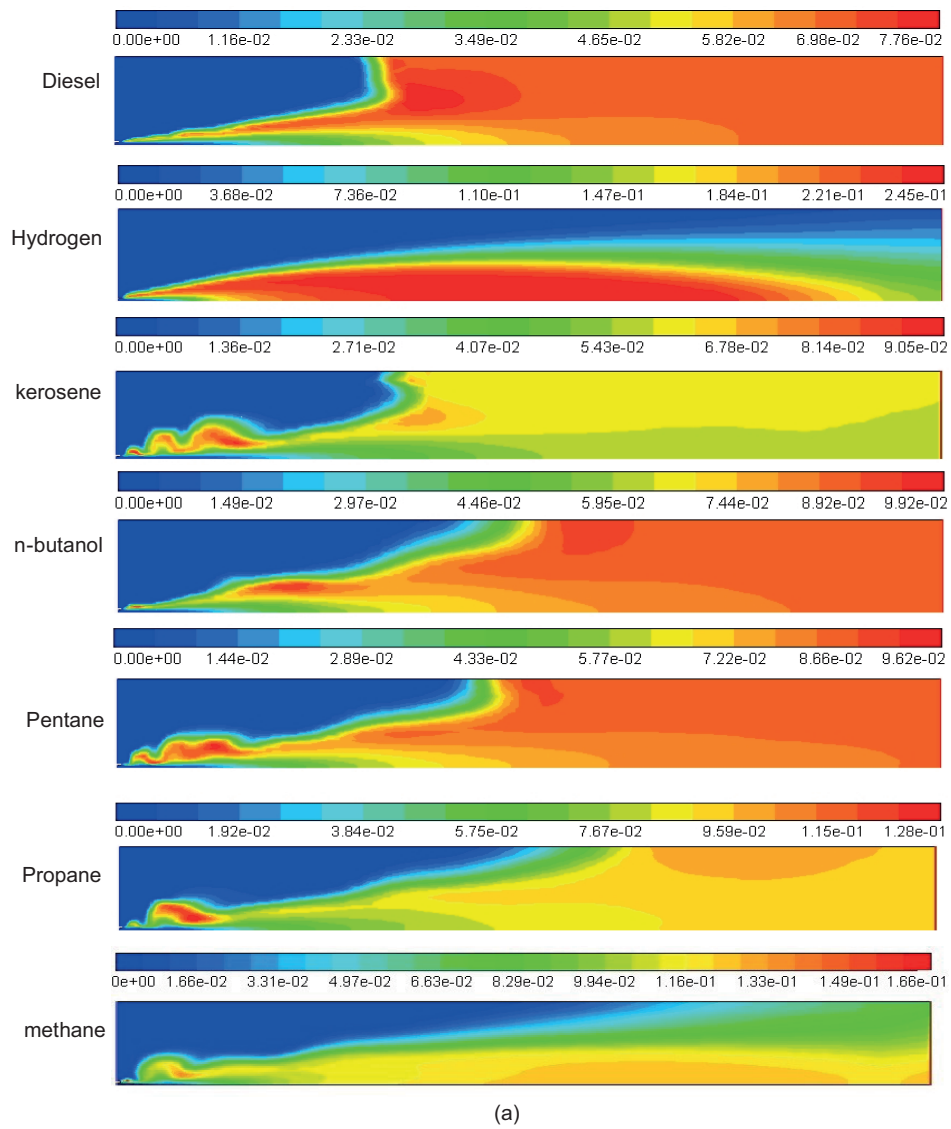
Figure 8. (a) Contours of H_2O pollutant inside domain with no radiation for diesel, hydrogen, kerosene, n-butane, pentane, propane and methane. (b) Maximum mass fraction of H_2O pollutant distribution in the combustion chamber for diesel, hydrogen, kerosene, n-butane, pentane, propane and methane.

(a)

(b)
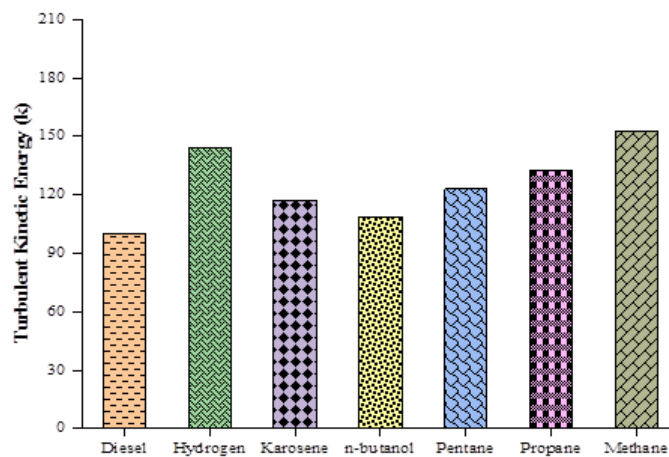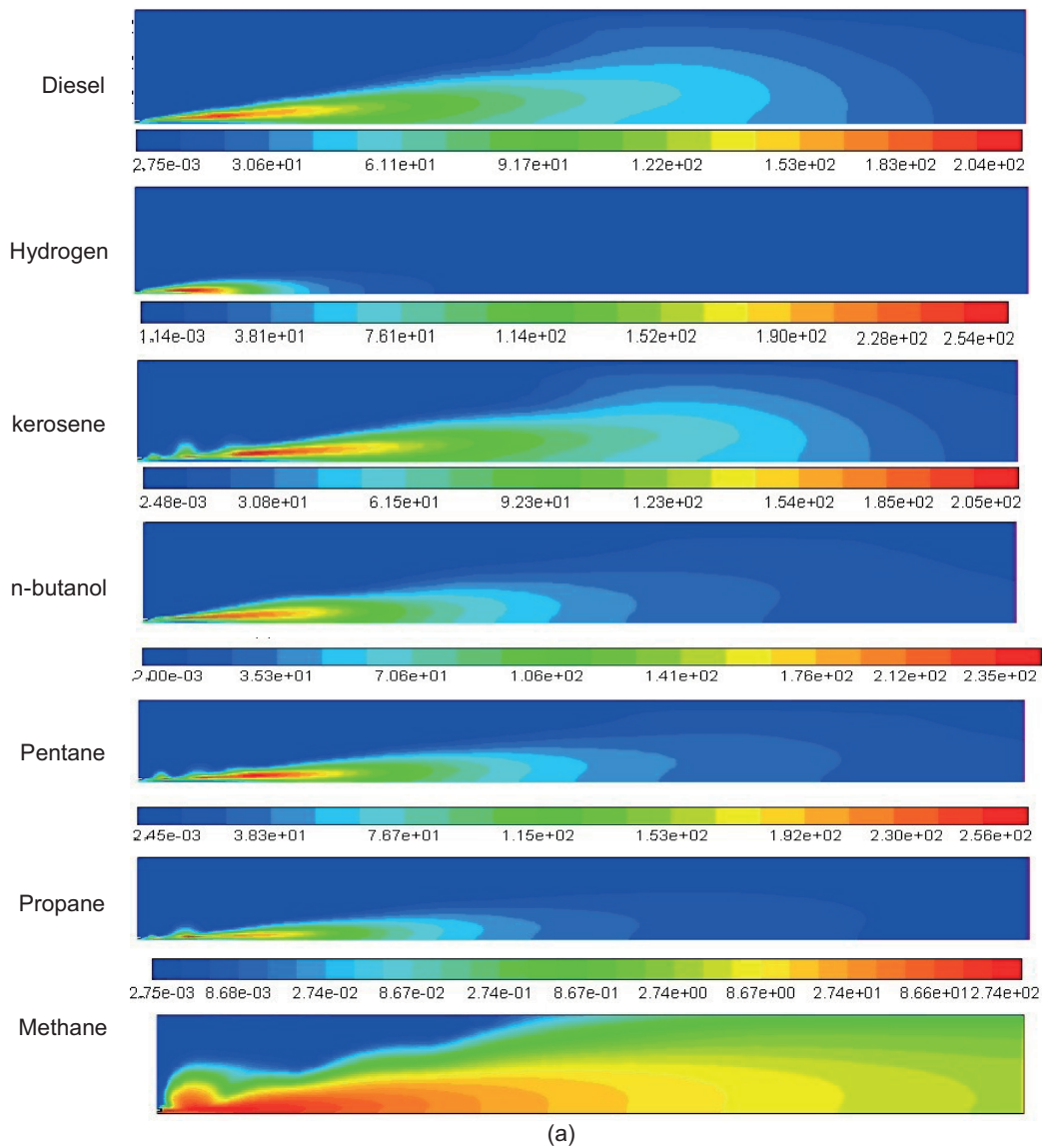
Figure 9. (a) Contours of TKE inside domain with no radiation for diesel, hydrogen, kerosene, n-butane, pentane, propane and methane. (b) Maximum turbulent kinetic energy for diesel, hydrogen, kerosene, n-butane, pentane, propane and methane.

kerosene fuel and lower for diesel fuel compared to other fuels. In the combustion chamber, TKE was found to be 100.04 for diesel fuel, 144.21 for hydrogen fuel, 117.21 for kerosene, 108.48 for n-butanol, 122.99 for pentane and 132.4 K, while in kerosene alternative fuel showed lowest mass fraction of H_2O emission than that of diesel fuel. Due to predictable diesel fuel is less viscous than alternative fuel.

CONCLUSION

In this paper the diesel, hydrogen, kerosene, n-butanol, pentane, propane and methane was determined by the species transport model for combustion characteristics and investigated in order to explore the promising solution to reduce the emissions of diesel engines.

- This study showed the significant effect of combustion cylinder geometry and evaluated emissions parameters operating with diesel, hydrogen, kerosene, n-butanol, pentane propane and methane fuels at constant flow rate.
- The overall patterns of variation in temperature, thermal and prompt NO, CO_2, O_2 and H_2O was suitably captured.
- A significant output is resulted by kerosene fuel on emissions reduction particularly prompt and thermal NO emission due to lower combustion cylinder temperature.
- The peak combustion cylinder temperature falls from 3800 K to 1800 K for hydrogen and 3500 K to 1690 K for kerosene.
- The CO_2 decreases with the hydrogen fuel compared to all the tested fuels.

Performance of different combustion fuels on diesel engine for emission reduction methods cannot be tried to undergo experimental procedure because of involvement of time period and price issue. Moreover, it decreases discharge exhaust gas emission up to lowest possible stage, which seems to be additional helpful in understandings of eco-friendly environmental characteristics. In this paper diesel-air, hydrogen-air, kerosene-air, n-butanol, pentane-air, propane-air and methane–air combustion fuels are taken to evaluate emissions characteristics.

ACKNOWLEDGMENT

NOMENCLATURE

x	The axial coordinate
r	The radial coordinate
v_x	The axial velocity, and
v_r	The radial velocity
P	The static pressure
$\bar{\bar{\tau}}$	the stress tensor
$\rho \vec{g}$	The gravitational body force
$\vec{F}$	External body force
s_m	mass added to the continuous phase from the dispersed second
G_k	Represents the generation of turbulence kinetic energy due to the mean velocity gradients
G_b	generation of turbulence kinetic energy due to buoyancy
Y_M	Represents the contribution of the fluctuating dilatation in compressible turbulence to the overall dissipation rate,
S_k	User Define Source
S_ε	User Define Source
$\bar{T}$	Average Temperature at outlet (K)
$\bar{v}$	Average velocity at outlet (m/s)
A	Area of cylindrical combustion chamber (m²)
U_T and τ_w	Friction velocity(m/s) and Local shear stress (N/m²)
K_v, E and $\sigma_{e,t}$	Von Karman constant, Wall Function and Turbulent Prandtl number
	Density (k/m³)
T and T_w	Temperature (K) and wall Temperature (K)
Y^+	Distance from the wall dimensionless
v	Kinematic viscosity (m²/S²)
C_p	Constant pressure Specific heat
σ_e	Laminar Prandtl number
Y	Distance from the wall
U^*	Velocity component to the wall
q_w	Wall heat flux

AUTHORSHIP CONTRIBUTIONS

Authors equally contributed to this work.

DATA AVAILABILITY STATEMENT

The authors confirm that the data that supports the findings of this study are available within the article. Raw data that support the finding of this study are available from the corresponding author, upon reasonable request.

CONFLICT OF INTEREST

ETHICS

There are no ethical issues with the publication of this manuscript.

REFERENCES

[1] Hosseini SM, Ahmadi R. Performance and emissions characteristics in the combustion of co-fuel diesel-hydrogen in a heavy duty engine. Appl Energy 2017;205:911–925. [CrossRef]

[2] Maes N, Skeen SA, Bardi M, Fitzgerald RP, Malbec L, Bruneaux G, et al. Spray penetration, combustion, and soot formation characteristics of the ECN Spray C and Spray D injectors in multiple combustion facilities. Appl Therm Eng 2020;172:115136. [CrossRef]

[3] Yousefi A, Birouk M. Investigation of natural gas energy fraction and injection timing on the performance and emissions of a dual-fuel engine with pre-combustion chamber under low engine load. Appl Energy 2017;189:492–505. [CrossRef]

[4] Yu H, Liang X, Shu G, Wang Y, Sun X. Numerical investigation of the effect of two-stage injection strategy on combustion and emission characteristics of a diesel engine. Appl Energy 2018;227:634–642. [CrossRef]

[5] An H, Yang W, Li J, Maghbouli A, Chua KJ, Chou SK. A numerical modeling on the emission characteristics of a diesel engine fueled by diesel and biodiesel blend fuels. Appl Energy 2014;130:458–465. [CrossRef]

[6] Zhao F, Yang W, Yu W, Li H, Sim YY, Liu T, et al. Numerical study of soot particles from low temperature combustion of engine fueled with diesel fuel and unsaturation biodiesel fuels. Appl Energy 2018;211:187–193. [CrossRef]

[7] Huang H, Zhu Z, Chen Y, Chen Y, Lv D, Zhu J. Experimental and numerical study of multiple injection effects on combustion and emission characteristics of natural gas – diesel dual-fuel engine. Energy Convers Manag 2019;183:84–96. [CrossRef]

[8] Kiat H, Gan S, Ng J, Mun K. Simulation of biodiesel combustion in a light-duty diesel engine using integrated compact biodiesel – diesel reaction mechanism. Appl Energy 2013;102:1275–1287. [CrossRef]

[9] Roman F, Vitorino C, França FHR. The influence of gas radiation on the thermal behavior of a 2D axisymmetric turbulent non-premixed methane – air flame. Energy Convers Manag 2014;79:405–414. [CrossRef]

[10] Oh J, Noh D, Ko C. The effect of hydrogen addition on the flame behavior of a non- premixed oxy-methane jet in a lab-scale furnace. Energy 2013;62:362–369. [CrossRef]

[11] Dixit S, Kumar A, Kumar S, Waghmare N, Thakur HC, Khan S. CFD analysis of biodiesel blends and combustion using ansys fluent. Mater Today Proceed 2020;26:665−670. [CrossRef]

[12] Johansson R, Leckner B, Andersson K, Johnsson F. Account for variations in the H 2 O to CO2 molar ratio when modelling gaseous radiative heat transfer with the weighted-sum-of-grey-gases model. Combust Flame 2011;158:893–901. [CrossRef]

[13] Silva CV, Vielmo HA, Alegre P. Combustion Science and Technology analysis of the turbulent, non-premixed combustion of natural gas in a cylindrical chamber with and without thermal. Combust Sci Technol 2014;179:1605−1630. [CrossRef]

[14] Soni DK, Gupta R. Optimization of methanol powered diesel engine: A CFD approach. Appl Therm Eng 2016;106:390–398. [CrossRef]

[15] Fluent Incorporated. Fluent theory guide. Canonsburg: ANSYS Inc.; 2015.

[16] Yadav R, Kushari A, Eswaran V, Verma AK. A numerical investigation of the Eulerian PDF transport approach for modeling of turbulent non-premixed pilot stabilized flames. Combust Flame 2013;160:618–634. [CrossRef]

[17] Rajak U, Nashine P, Verma TN. Characteristics of microalgae spirulina biodiesel with the impact of n-butanol addition on a CI engine. Energy 2019;189:116311. [CrossRef]

[18] Rajak U, Nashine P, Nath T, Pugazhendhi A. Performance and emission analysis of a diesel engine using hydrogen enriched n-butanol, diethyl ester and Spirulina microalgae biodiesel. Fuel 2020;271:117645. [CrossRef]

[19] Rajak U, Nashine P, Nath Verma T. Numerical study on emission characteristics of a diesel engine fuelled with diesel-spirulina microalgae-ethanol blends at various operating conditions. Fuel 2020;262:116519. [CrossRef]

[20] Krishania N, Rajak U, Kumar P. Investigations of spirulina, waste cooking and animal fats blended biodiesel fuel on auto-ignition diesel engine performance, emission characteristics. Fuel 2020;276:118123. [CrossRef]

[21] Rajak U, Nashine P, Verma TN. Effect of fuel injection pressure of microalgae spirulina biodiesel blends on engine characteristics. J Comput Appl Res Mech Eng 2021;11:113−125.

[22] Rajak U, Nashine P, Verma, TN. Effect of spirulina microalgae biodiesel enriched with diesel fuel on performance and emission characteristics of CI engine. Fuel 2020;268:117305. [CrossRef]

[23] Ahmadi N, Kõrgesaar M. Analytical approach to investigate the effect of gas channel draft angle on the performance of PEMFC and species distribution. Int J Heat Mass Transf 2020;152:119529. [CrossRef]

[24] Rezazadeh S, Ahmadi N. Numerical investigation of gas channel shape effect on proton exchange

membrane fuel cell performance. J Braz Soc Mech Sci Eng 2015;37:789–902. [CrossRef]

[25] Shankar S, Astagi HV, Hotti SR, Hebbal O. Effect of exhaust gas recirculation (EGR) on performance, emissions and combustion characteristics of a low heat rejection (LHR) diesel engine using Pongamia biodiesel. J Therm Eng 2016;2:1007–1016. [CrossRef]

[26] Abay K, Colak U, Yüksek L. Computational fluid dynamics analysis of flow and combustion. J Therm Eng 2018;4:1878–1895. [CrossRef]

[27] Gül MZ, Köten H, Yılmaz M, Savcı LH. Advanced numerical and experimental studies on CI engine emissions. J Therm Eng 2018;4:2234–2247. [CrossRef]

[28] Koten H. Performance analysis of a diesel engine within a multi. J Therm Eng 2018;4:2075–2082. [CrossRef]

[29] Rajak U, Nashine P, Verma TN. Effect of spirulina microalgae biodiesel enriched with diesel fuel on

performance and emission characteristics of CI engine. J Therm Eng 2020;268:117305. [CrossRef]

[30] Rajak U, Nashine P, Verma TN. Effect of fuel injection pressure in a diesel engine using microalgae-diesel Emulsion. Int J Eng Adv Technol 2019;8:263–271. [CrossRef]

[31] Koten H. Hydrogen effects on the diesel engine performance and emissions. Int J Hydrog Energy 2019;43:10511–10519. [CrossRef]

[32] Oztürk U, Hazar H, Yılmaz F. Comparative performance and emission characteristics of peanut seed oil methyl ester (PSME) on a thermal isolated diesel engine. Energy 2019;167:260–268. [CrossRef]

[33] Kurien C, Srivastava AK. Review on post-treatment emission control technique by application of diesel oxidation catalysis and diesel particulate. J Therm Eng, 2019;5:108–118. [CrossRef]

CORRIGENDUM

Corrigendum: A numerical investigation of the species transport approach for modeling of gaseous combustion

Upendra RAJAK,[1] Prem KUMAR CHAURASIYA[2], Prerana NASHINE[3] Rohit KUMAR,[2] Tikendra NATH VERMA[4]

[1]*Department of Mechanical Engineering, Rajeev Gandhi Memorial College of Engineering and Technology Nandyal-518501, India*
[2]*Department of Civil Engineering, Madan Mohan Malaviya University of Technology Technical University Gorakhpur- 273016, India*
[3]*Department of Mechanical Engineering, Sagar Institute of Science and Technology Gandhi Nagar, Bhopal, M.P, India*
[4]*Department of Mechanical Engineering, Maulana Azad National Institute of Technology Bhopal-462003, India*

CORRIGENDUM

J Ther Eng Vol. 7, Supp 14, pp. 2054-2067

The list of the authors was incomplete in the original publication.

The correct list is:

Upendra RAJAK, Prem KUMAR CHAURASIYA, Prerana NASHINE, Rohit KUMAR, Tikendra NATH VERMA

*Corresponding author.
*E-mail address: upendrarajak86@gmail.com; verma.tikks@gmail.com